Radiation Measurements 173 (2024) 107097

Contents lists available at ScienceDirect

Radiation Measurements

journal homepage: www.elsevier.com/locate/radmeas

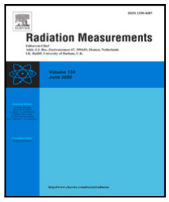

Converter thickness optimisation using Monte Carlo simulations of Fluorescent Nuclear Track Detectors for neutron dosimetry

Stefan Schmidt [a,b,c,d,e,*], Alberto Stabilini [f], Long-Yang J. Thai [a,b,c,g], Eduardo G. Yukihara [f], Oliver Jäkel [b,c,d], José Vedelago [a,b,c]

[a] Department of Radiation Oncology, Heidelberg University Hospital (UKHD), Heidelberg, Germany
[b] Department of Medical Physics in Radiation Oncology, German Cancer Research Center (DKFZ), Heidelberg, Germany
[c] Heidelberg Institute for Radiation Oncology (HIRO), National Center for Radiation Research in Oncology (NCRO), Heidelberg, Germany
[d] Medical Faculty Heidelberg, Heidelberg University, Heidelberg, Germany
[e] Heidelberg Ion Beam Therapy Center (HIT), Heidelberg University Hospital, Heidelberg, Germany
[f] Department of Radiation Safety and Security, Paul Scherrer Institute (PSI), Villingen, Switzerland
[g] Department for Physics and Astronomy, University of Heidelberg, Heidelberg, Germany

ARTICLE INFO

Keywords:
Fluorescent nuclear track detectors
Neutron dosimetry
Converter thickness
Detector sensitivity
Monte Carlo simulations

ABSTRACT

Secondary neutrons generated during ion beam radiotherapy present a concern due to the potential dose deposition beyond the treatment volume, thereby elevating the risk of inducing secondary tumours. These neutrons can possess energies comparable to those of the primary ions, reaching magnitudes of several hundred MeV, posing a challenge for neutron detectors. Fluorescent Nuclear Track Detectors (FNTDs) are promising detectors for high-energy neutron dosimetry given their capability to detect particles with a low linear energy transfer. In this work, the sensitivity of FNTDs to neutron energies reaching 20 MeV was analysed by experiments and Monte Carlo (MC) simulations, quantifying the recoil proton yield of FNTDs combined with polyethylene (PE) converters of different thicknesses. The FNTDs were read out using a dedicated FNTD reader, demonstrating a reasonable uncertainty by analysing a detector area of 0.1 mm^2. Investigations of different converter thicknesses reveal optimal detector sensitivity between 0.5 mm to 1.0 mm for a ^{241}AmBe source, yielding a maximum sensitivity of (22.7±3.4) tracks mSv^{-1} mm^{-2}. Similar converter-FNTD configurations were assessed through MC simulations using FLUKA, yielding a correlation between detector sensitivity and converter thickness. Furthermore, an enhanced detector sensitivity for neutron energies up to 20 MeV was found for the PE converter thickness of 4.0 mm. The MC simulations can be used to optimise FNTD detector configurations for measuring higher neutron energies by maximising the recoil proton yield.

1. Introduction

Cancer is a leading cause of mortality, rendering radiotherapy an essential treatment modality for patients. Ion beam radiotherapy (IBRT) using protons and light ions represents a treatment type suitable for certain indications and tumour locations, particularly central nervous system tumours, sarcomas such as chordomas and paediatric tumours (Dreher and Combs, 2018). IBRT enables precise targeting of the tumour by exploiting the well-defined range of particles at a given energy, known as the Bragg peak, allowing highly conformal radiotherapy while sparing normal tissue (Wilson, 1946; Jäkel et al., 2022). In addition, particles heavier than protons possess a higher biological effectiveness, which can enhance the therapy outcome even for radioresistant tumours (Scholz, 2000; Schardt et al., 2010).

A potential issue in IBRT is the generation of secondary neutrons, significantly contributing to out-of-field dose and carrying the potential risk of inducing secondary cancers outside the treated volume (Schneider and Hälg, 2015; Smith et al., 2019). Notably, IBRT can produce secondary neutrons with energies similar to those of the primary ions, reaching several hundred MeV (Shrestha et al., 2022; Van Hoey et al., 2022; Vedelago et al., 2022; Geser et al., 2024). At these high neutron energies, achieving precise dose estimation has been hampered by the limited detection sensitivity exhibited by certain neutron detectors (Mayer et al., 2006; Gómez-Ros et al., 2023). Furthermore, some active detectors such as rem counters are suitable for high neutron energies up to GeV, but they are not suitable for personal dosimetry or in-phantom measurements (Olsher et al., 2000; Toppi et al., 2020). Similarly, thermoluminescence detectors are only suitable for thermal

* Corresponding author at: Department of Radiation Oncology, Heidelberg University Hospital (UKHD), Heidelberg, Germany.
E-mail address: stefan.schmidt@dkfz.de (S. Schmidt).

https://doi.org/10.1016/j.radmeas.2024.107097
Received 21 December 2023; Received in revised form 7 March 2024; Accepted 14 March 2024
Available online 16 March 2024

neutrons, although the energy range can be extended by relying on albedo neutrons back-scattered by the body (ICRU, 2002; Gambarini et al., 2004). Plastic Nuclear Track Detectors (PNTD) are widely used in neutron personal dosimetry and can be used up to several MeV (Tanner et al., 2005). However, for energies beyond 10 MeV, their response function does not follow the recommended fluence-to-ambient dose conversion coefficient curve, imposing limitations for the energies of secondary neutrons produced in IBRT facilities (Domingo et al., 2013).

Fluorescent Nuclear Track Detectors (FNTDs) offer suitable characteristics for neutron dosimetry including small detector size, non-destructive readouts and re-usability after bleaching (Akselrod and Kouwenberg, 2018). They also exhibit capability for Linear energy transfer (LET) measurements down to $0.4\,\mathrm{keV\,\mu m^{-1}}$, capturing recoil protons generated by high-energy neutrons up to several hundred MeV (Akselrod et al., 2006; Sykora et al., 2008a).

One option to characterise the response of the detector is to use computational tools for simulations. The Monte Carlo (MC) code FLUKA (Fluktuierende Kaskaden), along with its graphical user interface FLAIR, was employed as a radiation transportation code (Vlachoudis, 2009; Battistoni et al., 2015; Ahdida et al., 2022). It can be used to simulate interactions between particles and matter, including neutrons across a broad energy spectrum. MC simulations are particularly relevant for higher energy neutrons since the available facilities offering neutron fields with energies above the ^{241}AmBe are scarce (Pomp et al., 2013; Colonna et al., 2018).

Studies based on MC simulations have been conducted for FNTDs with neutrons up to 140 MeV, revealing the detector response and sensitivity to high-energy neutrons (Wang et al., 2019; Stabilini et al., 2021b). Additional experimental data is needed to completely characterise FNTDs within these energy ranges. There have been some experimental studies, but primarily for neutrons possessing lower energies, ranging from a few MeV up to almost 20 MeV. However, these studies focused on aspects such as the neutron energy dependence of FNTDs for neutron energy determination (Sykora et al., 2009; Fomenko et al., 2018).

This study investigates the optimisation of the converter thickness to enhance FNTD sensitivity for neutron dosimetry. The presented methodology aims to maximise the generation of recoil protons. To achieve this, the sensitivity of FNTDs was analysed for four distinct polyethylene (PE) converter thicknesses between 0.5 mm and 3.0 mm. A ^{241}AmBe neutron source was used for the irradiations, followed by imaging using a dedicated FNTD reader. The detector response was also quantified using MC simulations to estimate the converter thicknesses for neutron energies of up to 20 MeV.

2. Materials and methods

2.1. Detectors and irradiations

FNTDs manufactured by Landauer Inc. (Stillwater, OK, USA) were used, with dimensions of $8.0\,\mathrm{mm} \times 4.0\,\mathrm{mm} \times 0.5\,\mathrm{mm}$ respectively in length, width and height, and polished to optical quality on one side (lot number #144004, process date 21.12.2020).

In-house manufactured neutron converters were employed to generate recoil protons that create ionisation tracks in the FNTDs. The converter used in this study consists of high-density PE purchased from Merck KGaA (Darmstadt, Germany; product number GF29956461-1EA) with a density of $0.95\,\mathrm{g\,cm^{-3}}$, which induces elastic scattering of the neutrons at the hydrogen atoms (Sykora and Akselrod, 2010).

For precise measurements, the FNTDs were placed on a 3D-printed holder on top of the converter materials. The holder guarantees a fixed distance between the source and converter surface of 0.46 mm, as it was done previously (Becker et al., 2022). A total of four converters with thicknesses of 0.5 mm, 1.0 mm, 2.0 mm and 3.0 mm were used. Fig. 1 displays a sketch of the converter-detector arrangement. The manufacturing of the converter has been done with an accuracy of 0.1 mm, owing to the precision of the converter material cutting. Additionally, the holder has an uncertainty of 16 µm due to 3D printing.

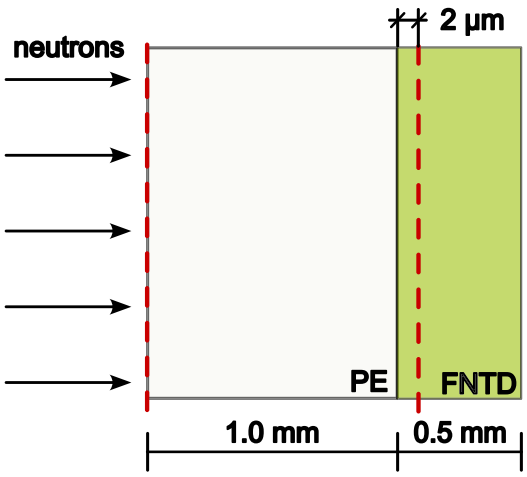

Fig. 1. Experimental setup for a 1.0 mm thick PE converter with the 0.5 mm thick FNTD. The primary neutrons impinge from the left-hand side. The two scoring planes for the MC simulations are highlighted by the two red dashed lines, the first for scoring the neutron fluence reaching the PE and the second (not to scale) for scoring the recoil proton fluence inside the FNTD.

The ^{241}AmBe source is one of the standard neutron sources used as a reference for detector-response characterisation and calibration (Vanhavere et al., 1998; Yukihara et al., 2017). Thus, irradiations were conducted at the German Cancer Research Centre (DKFZ; Heidelberg, Germany) using a ^{241}AmBe source with a nominal activity of 37 MBq and associated uncertainty of ±10 %. The ^{241}AmBe source, with a diameter of 17.4 mm and a height of 19.2 mm, has a fluence-averaged energy of 4.17 MeV and a maximal energy of 11 MeV (ISO 8529-1:2021-11, 2021). It is packed in an X.2 capsule and has been calibrated at the Physikalisch-Technische Bundesanstalt (PTB; Braunschweig, Germany). The gamma-ray background due to the packing of the source is less than 3.5 % (ISO 8529-1:2021-11, 2021). Irradiations of single FNTDs were performed for ambient dose equivalent $H^*(10)$ values of 10 mSv, 50 mSv, 100 mSv, 150 mSv, 200 mSv, 250 mSv and 300 mSv.

2.2. Readout procedure and track counting

FNTDs were read out using a dedicated confocal laser scanning microscope, the FXR700RG from Landauer (Akselrod et al., 2014). This device allows fully automated reading of up to 216 FNTDs, including automatic surface detection and the ability to capture stacked images, thus allowing high throughput of detectors. The output from the FNTD reader, in either image or text file format, contains information on the intensity distribution across the acquired area. The parameters for readout were configured for a field size of $100\,\mu\mathrm{m} \times 100\,\mu\mathrm{m}$, a resolution of $512\,\mathrm{px} \times 512\,\mathrm{px}$, a scan depth of 2 µm and an imaging time of 100 s.

Fiji (version 1.54f), a successor to ImageJ, was used to identify the recoil proton tracks in the images through a dedicated FNTD plugin (Schindelin et al., 2012; Klimpki et al., 2016). Its core element is the MOSAIC package, which allows background corrections to be applied to the raw image, as well as the identification of potential track spots (Sbalzarini and Koumoutsakos, 2005).

Intra- and inter-detector sensitivity differences due to differences in colouration must be corrected before comparing different images (Klimpki et al., 2016). Becker et al. (2022) presented a so-called intensity threshold variation method, which is also used here. The basic idea of this method is to determine a user-independent intensity threshold parameter t^*, which is later used for the tracking algorithm to remove false-true track spots. Briefly, the relation between the variable threshold parameter t and the number of identified tracks results in a similar curve shape for all images, thus two regions can be identified

and fitted with a linear model. One region describes the overestimation and the other the underestimation of identified tracks. By calculating the intersection of the linear fits from each region, the t^* value can be determined.

As the t^* methodology described was developed for a multipurpose confocal microscope, the same FNTD samples from the previous study were analysed using the FNTD reader. The results, shown in the supplementary material, showed good agreement and allowed the post-processing procedures to be transferred to images acquired with the FNTD reader. To adapt the original t^* procedure to the output of the FNTD reader, some adjustments were necessary. These adjustments include increasing the minimum number of data points required for the linear fit in the underestimation region, thus accounting for the greater data variability with the FNTD reader. Additionally, the fitting procedure in the overestimation region was adjusted by redefining parameter and offset values, as the post-processing tended to initiate the linear fit before the defined overestimation region, resulting in a smaller value of t^*. Moreover, the process was further automated by using the Python scripting functionality in Fiji. Subsequently, Matlab 2023a (MathWorks, Natick, Massachusetts, USA) was employed for post-processing routines (The MathWorks Inc., 2023). The new version of the t^* code is included as supplementary material.

2.3. Uncertainty analysis

Two main sources of uncertainty have been identified during the track counting procedure. The first contribution comes from the characteristic neutron emission from the ^{241}AmBe source, leading to a dispersion in the number of tracks for different readout fields, called $u(source)$. It was quantified using the standard deviation of the mean number of identified tracks in the readout fields, representing the systematic uncertainty. The other major contribution comes from the t^* methodology, called $u(t^*)$, and represents the statistical uncertainty (GUM 2008). It was quantified by the uncertainties associated with the linear fits used to determine the t^* value. The determination of the intersection point reveals an uncertainty $u(int)$, which is used to determine the number of tracks for the lower uncertainty bound, yielding a $u(int)$ for each scanned field. By using gaussian uncertainty propagation, the uncertainty of the t^* methodology can be calculated for a given number of readout fields n as specified in Eq. (1):

$$u(t^*) = \frac{1}{n}\sqrt{\sum_{i=1}^{n} u(int)_i^2} \tag{1}$$

where the index i iterates through the different readout fields. Considering these two uncertainty contributions, the total uncertainty can be calculated according to Eq. (2):

$$u(total) = \sqrt{u(t^*)^2 + u(source)^2} \tag{2}$$

2.4. Monte Carlo simulations and sensitivity calculation

MC simulations were performed with FLUKA (version 4-3.4) embedded in the Flair (version 3.2-4) environment (Vlachoudis, 2009; Battistoni et al., 2015; Ahdida et al., 2022). One of the major changes introduced in the FLUKA version 4-3.0 is the pointwise neutron transport below 20 MeV (Mendoza et al., 2012, 2014; Mendoza and Cano-Ott, 2018). The energies were sampled from a custom FLUKA user routine, using the energy spectrum of a ^{241}AmBe source according to the ISO 8529-1 (ISO 8529-1:2021-11, 2021). The source was implemented as a 3D cylindrical volume and an isotropic angular distribution of neutrons was simulated in agreement with the experimental setup. The neutron fluence was scored at the PE converter surface and the proton fluence at a depth of 2 µm within the FNTD using unidirectional USRBDX scoring cards. A scoring area of 16 mm^2 was used for both protons and neutrons, corresponding to the FNTD covered with PE as in the experimental setup. A visualisation of the geometry and the scoring positions can be found in Fig. 1.

Table 1
Fluence-to-ambient dose equivalent conversion coefficient f. For *, the spectrum-averaged value for the ^{241}AmBe source is given, and for $^+$, the values are obtained by cubic interpolation between the tabled values (ICRP, 1996).

Neutron energy (MeV)	f factor (pSv cm^2)
4.17*	391
5.0	408
8.0	409
14.8	536.3$^+$
19.0	584.6$^+$

The comparison between simulations and experiments is done by comparing the sensitivity values obtained by the two methods. For the experiments, the sensitivity C_{PE} (tracks mSv^{-1} cm^{-2}) can be derived directly from the calibration curve as the slope of the linear fit. Instead, the simulated sensitivity needs to be computed according to Eq. (3), taking into account the proton fluence ϕ_p (primary^{-1} cm^{-2}) at 2 µm depth within the FNTD and below the PE converter as well as the neutron fluence ϕ_n (primary^{-1} cm^{-2}) at the converter surface (Stabilini et al., 2021b):

$$c_{PE} = \frac{\phi_p * 10^9}{\phi_n * f} \tag{3}$$

where f is the fluence-to-ambient dose conversion coefficient (pSv cm^2), tabulated for the energies used in this study in Table 1 (ICRP, 1996). The conversion from pSv to mSv is done with the factor 10^9 in Eq. (3). The uncertainty of the simulations is derived from the propagation of uncertainty in Eq. (3).

In the simulations, the fluences were scored double differentially in energy and angle using the USRBDX card. In addition, the USRBIN card was used for scoring the spatial distribution of the fluence in a cartesian mesh. This way, the proton fluence was first estimated with the USRBIN card at the surface of the FNTD, followed by the sensitivity value estimation with the resulting converter thickness at a depth of 2 µm using the USRBDX card.

In the next stage, further measurements at higher neutron energies are planned to assess the converter optimisation methodology. Therefore, simulations of the mono-energetic ISO reference neutron fields available at PTB[1] were conducted for neutron energies ranging from 5 MeV to 20 MeV, as reported in Table 1 (Nolte et al., 2004).

3. Results

3.1. Optimisation of the readout area for the FNTD reader

To identify the optimal number of readout fields or equivalently the FNTD area necessary for reducing uncertainty, an examination was performed across various sizes of readout area quantifying the mean number of identified tracks and their corresponding uncertainties. Fig. 2a shows the mean number of identified tracks as a function of the readout area up to 0.30 mm^2 for two FNTD samples irradiated with 10 mSv and 300 mSv, using the 1.0 mm thick converter. The reported values are normalised to the mean number of identified tracks at 0.10 mm^2, which is 5480 tracks mm^{-2} for 10 mSv and 12 322 tracks mm^{-2} for 300 mSv. For both data sets, the mean values are overestimated by more than 20 % for the smaller readout areas, and its deviation decreases below 5 % of the normalised value after 0.05 mm^2. Moreover, for readout areas larger than 0.10 mm^2, the deviation remains within ± 5 % of the mean value for both detectors.

[1] The PTB facility offers reference fields of mono-energetic neutron beams. The highest energy neutron beam available is 19 MeV, therefore this value was used for the MC simulations. Nevertheless, for the general text like the introduction, the nominal value of 20 MeV is used, since it is the one usually reported in other publications.

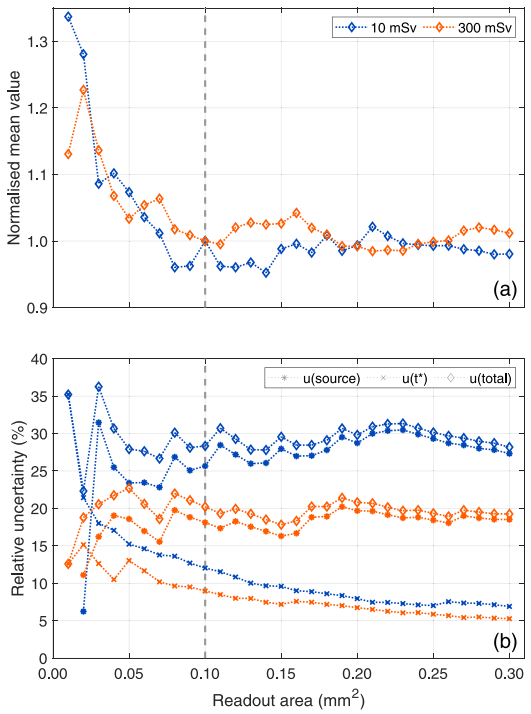

Fig. 2. Optimal readout area for the FNTD reader: (a) mean number of tracks and (b) the corresponding uncertainties as a function of the readout area. The two contributions as well as the total uncertainty are plotted. Lines connecting the dots are plotted for visual aid.

Fig. 2b presents the total uncertainty $u(total)$ and the two contributions to it, $u(source)$ and $u(t^*)$, also as a function of the readout area. For the smallest readout area, which corresponds to only one readout field, there is no data point for $u(source)$ because the variance and thus the standard deviation equals per definition zero. For both samples, a decrease in $u(t^*)$ is evident during the initial increase of the readout area. Within the range spanning from 0.10 mm^2 to 0.30 mm^2, the uncertainty decreased respectively from 12.0 % to 6.9 % for the FNTD irradiated with 10 mSv and from 9.0 % to 5.3 % for the FNTD irradiated with 300 mSv. Instead, $u(source)$ presents some fluctuations for the smaller areas, reaching a steady trend with changes between 26 % to 31 % for the 10 mSv and 16 % to 20 % for the 300 mSv sample. Increasing the readout area from 0.10 mm^2 to 0.30 mm^2 reduced the total uncertainty by less than 1 % according to the values obtained for both samples, representing no significant improvement.

Taken together, the results reveal that an analysis encompassing a readout area of 0.10 mm^2 with the FNTD reader could strike a balance between accuracy and the extent of post-processing effort, thereby increasing the overall readout process efficiency. This is based on two main facts observed in Fig. 2 for both samples: (i) the mean number of identified tracks for 0.10 mm^2 is not significantly changing when increasing the scanned area; (ii) $u(total)$ at 0.10 mm^2 is already dominated by $u(source)$ with a similar value compared to the largest area, while $u(t^*)$ steadily decreases without any major impact. Hence, further results were obtained by analysing this specific FNTD area.

3.2. Effect of converter thickness on the sensitivity to the ^{241}AmBe source

To examine the correlation between converter thickness and FNTD sensitivity, detectors equipped with various converter thicknesses were exposed to a ^{241}AmBe radiation source, followed by establishing a calibration curve to derive sensitivity values. Fig. 3 depicts the calibration curves for converters with thicknesses of 0.5 mm, 1.0 mm, 2.0 mm and 3.0 mm. For all four converters, the mean values of the identified tracks exhibit an ascending trend with the increase in dose.

Table 2
Detector sensitivities and coefficient of determination for different converter thicknesses.

Converter thickness (mm)	Sensitivity (tracks mSv^{-1} mm^{-2})	R^2
0.5	19.6 ± 2.4	0.931
1.0	22.7 ± 3.4	0.897
2.0	20.0 ± 1.3	0.981
3.0	19.4 ± 2.0	0.948

A weighted linear regression was employed to determine the slopes for each calibration curve, corresponding to the sensitivity of the detector. The sensitivity of each fit along with the coefficient of determination R^2 are summarised in Table 2. The values indicate that the detector sensitivity first increases with increasing converter thickness and reaches its maximum at a converter thickness of 1.0 mm for the ^{241}AmBe source. According to the trend of the mean values, a further increase in converter thickness leads to a decrease in sensitivity.

3.3. Monte Carlo simulations for the ^{241}AmBe

MC simulations using FLUKA were conducted to determine the sensitivity values across different converter thicknesses and compared to the experimental results for validation. Fig. 4 displays the results of both the simulation and experimental investigation. It is worth mentioning that the experimental data has uncertainties in the converter and holder dimensions of 0.1 mm and 0.016 mm, respectively, which are represented by the horizontal error bars. Furthermore, the resolution of the experimental data is restricted as it only contains two data points describing the region for converter thicknesses of 1.0 mm and smaller. Overall, simulations and experiments both agree with a maximum deviation of 28 %. They follow a similar trend of increasing sensitivity, followed by a decrease when increasing the converter thickness.

The simulations yielded the highest sensitivity values for a converter thickness of 0.5 mm, corresponding to (25.3 ± 0.3) tracks mSv^{-1} mm^{-2}. Instead, a maximum sensitivity of (22.7 ± 3.4) tracks mSv^{-1} mm^{-2} was observed for a converter thickness of 1.0 mm based on the experimental data. Although the data points for converter thicknesses below 1.0 mm and above 2.0 mm deviate, the findings reveal a correlation between sensitivity and converter thickness for both simulations and experimental data. Based on the results for the ^{241}AmBe source, the MC model was used to estimate the converter thickness and detector sensitivity. A deeper discussion on the discrepancy between simulations and experiments is presented in Section 4.2.

3.4. Monte Carlo study on converter thickness and detector sensitivity for higher neutron energies

To ascertain the optimal thickness for the converter to detect high-energy neutrons, MC simulations were performed for different converter thicknesses. The findings are depicted in Fig. 5a. The proton fluence increases initially for all energies analysed until it reaches a maximum at a specific depth, after which the fluence decreases. Between the converter thickness at which proton fluence is maximal and a converter thickness of 10.0 mm, the proton fluence decreases by less than 10 %. From the observation of the four different curves, it is notable that increasing neutron energy requires a thicker neutron converter to achieve maximum proton fluence.

For these four curves, the converter thickness that gives the maximum proton fluence was identified with the USRBIN card and dedicated simulations were performed using the USRBDX card to assess the detector sensitivity for these converter thicknesses. Fig. 5b illustrates the outcomes, which reveals a detector sensitivity of (38.5 ± 0.2) protons primary^{-1} mm^{-2} for the mono-energetic 5 MeV beam when using a converter of 0.6 mm thickness. The sensitivity for neutrons with an energy of 19 MeV is almost 2.5 times greater than for neutrons with

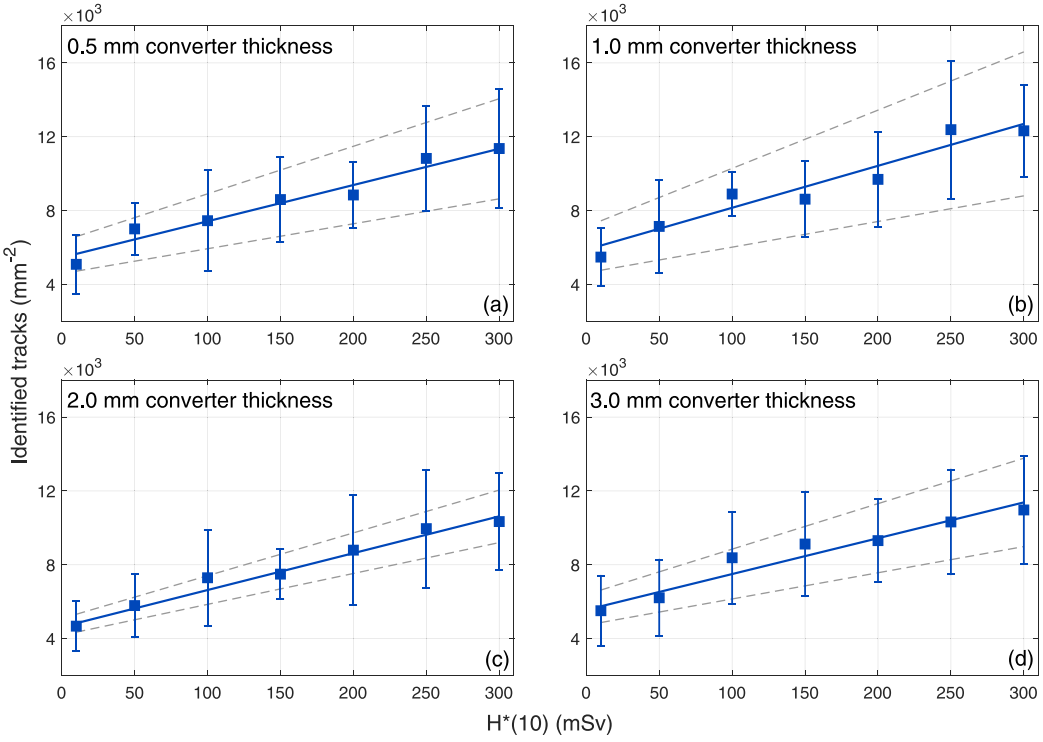

Fig. 3. Influence of converter thickness on the FNTD sensitivity. Obtained calibration curves for (a) 0.5 mm, (b) 1.0 mm, (c) 2.0 mm and (d) 3.0 mm converter thickness. The mean number of identified tracks for each dose is indicated as a blue square with the error bars as $u(total)$. The solid lines represent each linear fit and the dashed lines the 95 % confidence interval.

an energy of 5 MeV. To achieve this sensitivity, the required converter thickness is 4.0 mm, which is more than 6 times greater than the thickness required for neutrons with an energy of 5 MeV. The slower rise in sensitivity at higher neutron energies is due to the declining cross-section of elastic interactions between neutrons and matter, thereby leading to a diminished rate of recoil proton generation. This MC-based investigation showcased the potential for enhanced detector sensitivity at higher neutron energy levels by enlarging the converter thickness.

4. Discussion

4.1. Readout area and uncertainty estimation

In this study, the effect of increasing the readout area has been analysed with a focus on the dedicated FNTD reader. It has been shown that the total uncertainty is dominated by the uncertainty associated with the neutron source. This effect might be related to the nature of neutron emissions since it cannot be compensated by increasing the readout area and agrees with the uncertainty of the ^{241}AmBe source reported in the calibration document (ISO 8529-1:2021-11, 2021). However, a deeper analysis of Fig. 2b suggests that there may also be a statistical contribution to $u(source)$ related to the absolute dose value, which is represented by the absolute number of tracks, resulting in a smaller $u(source)$ for the 300 mSv FNTD in comparison to the 10 mSv FNTD. At the same time, the uncertainty of the t^* methodology has a minor impact on the total uncertainty, particularly when the field size increases from 0.10 mm^2 to 0.30 mm^2. Therefore, it can be concluded that with this readout procedure, a readout area of 0.10 mm^2 is sufficient for the track determination to ensure that the mean number of track value remains within ±5 %.

However, it has been presented that the readout area required for FNTD analysis varies depending on the post-processing procedure and the microscope image quality. While Sykora and Akselrod (2010) implemented 45 to 150 readout fields of 0.01 mm^2 each, Becker et al. (2022) employed one single readout field of 0.0182 mm^2 with a higher

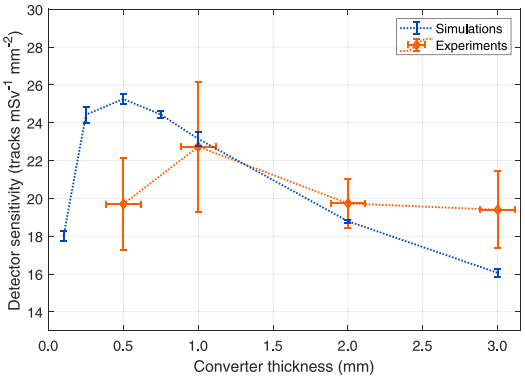

Fig. 4. FNTD detector sensitivity for different converter thicknesses, comparing experimental data and data obtained from MC simulations. The dashed lines connecting the markers are plotted for visual aid.

image quality. In the former work, the observed sensitivity was stated with an uncertainty of about 8.1 %, while in the latter, the dose value was specified with an uncertainty of about 9.4 % on average, compared to a mean uncertainty of 11.0 % according to the values reported in Table 2.

The uncertainties reported in Fig. 2 can be further decreased by increasing the number of FNTDs irradiated per dose value, as demonstrated in the supplementary material. For instance, for the 1.0 mm converter, computing the linear fit with the irradiations done in triplicate leads to a sensitivity relative uncertainty of 2.2 %, compared to the 15.0 % reported in Table 2. Since the goal of this study was to evaluate the impact of various converter thicknesses, comparing mean values is adequate.

An offset of the calibration curves was found, consistent with earlier research (Becker et al., 2022). This offset may have resulted from the post-processing procedure and the absence of specific corrections for the gamma contribution. Nevertheless, the offset appears

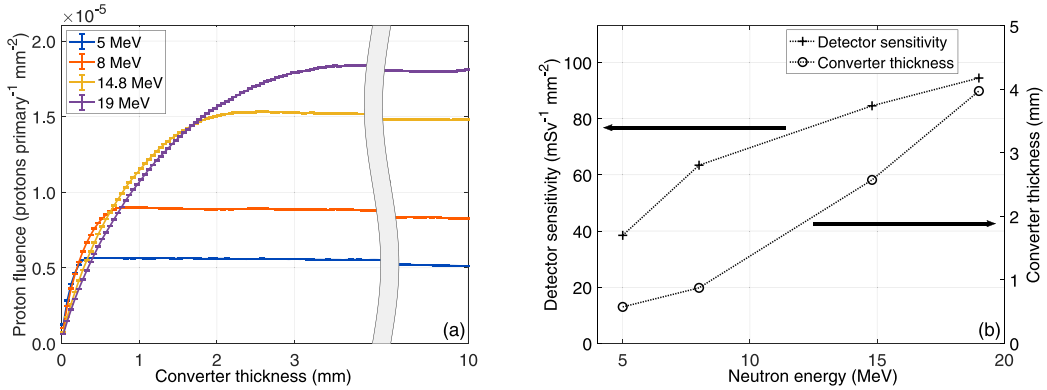

Fig. 5. Monte Carlo study of the optimisation of converter thickness for higher neutron energies. (a) Proton fluence as a function of converter thickness. (b) Maximal detector sensitivity at 2 μm depth of the FNTD and corresponding converter thickness. As the uncertainties are smaller than the marker size, the error bars are not displayed. In both plots, the dots are connected with lines for visual aid.

to be unrelated to the absolute dose values because the obtained slope of (22.7 ± 3.4) tracks mSv^{-1} mm^{-2} for the 1.0 mm thick converter presents no significant difference from the ones reported in other studies. For instance, Becker et al. (2022) reported a slope of (21.1 ± 2.0) tracks mSv^{-1} mm^{-2}, while Akselrod et al. (2006) reported (21.0 ± 4.0) tracks mSv^{-1} mm^{-2}. Thus, the presented analysis is valid in terms of maximising the recoil proton yield for different converter thicknesses.

4.2. Influence of converter thickness on sensitivity for the ^{241}AmBe source

The analysis of the converter thickness revealed an increase in sensitivity with increasing converter thickness and a decrease in sensitivity after reaching an optimum converter thickness (Table 2 and Fig. 3). The increase in sensitivity is explained by the build-up effect due to the formation of recoil protons with increasing depth inside the PE converter. When the same number of recoil protons are created and stopped inside the converter, maximum sensitivity is reached in the detector. The subsequent decrease in sensitivity is mainly due to the decrease in neutron fluence. Notably, a similar discussion applies to the higher neutron energies reported in Fig. 5a.

It was possible to reproduce the main results of the experimental part using the FLUKA MC code, yielding comparable sensitivity values, as reported in Fig. 4. A deviation of 4.8 % was found between the mean value of the simulation compared to the experiment for the 2 mm converter thickness, in agreement with previous studies for FNTDs presenting deviations of 5.6 % for the same converter thickness (Stabilini et al., 2021b).

For the 1.0 mm and 2.0 mm thick converters, the sensitivity values observed in both experiments and simulations fall within the range of the associated uncertainties. However, a discrepancy was found for the other experimental values compared to the simulations. One source of uncertainty contributing to the discrepancy might be the 0.1 mm uncertainty in the manufacture of the converters, combined with the relatively reduced discrete values quantified experimentally. Further analysis of the discrepancy could be achieved by reducing uncertainty in the experimental setup or by using different MC codes.

Overall, the results from the simulations align with the experimental sensitivities in terms of trend and magnitude and are therefore used to optimise the converter thickness. The MC study on the impact of converter thickness at higher neutron energies is not expected to be significantly influenced by the discrepancies observed previously, as it only indicates the trend of proton fluence and sensitivity. However, it is essential to experimentally calibrate the response of the detectors with the optimised converter for accurate neutron dose assessment, because of the discrepancies of up to 28 % between the absolute sensitivity values in simulations and experiments.

4.3. Mono-energetic neutrons versus broad neutron spectrum

For the simulation of mono-energetic neutrons with energies of 5 MeV, it has been shown that similar trends and behaviour can be expected as for the ^{241}AmBe experiments. For the ^{241}AmBe, where the mean neutron energy is 4.2 MeV, a PE converter with a thickness between 0.5 mm to 1.0 mm maximise the sensitivity. This is in agreement with the required thickness for 5 MeV, shown in Fig. 5b. The 5 MeV mono-energetic neutrons exhibit greater sensitivity due to their ability to generate recoil protons with a longer range compared to the fraction of lower energy neutrons originating from the ^{241}AmBe (ISO 8529-1:2021-11, 2021).

Many studies have analysed the recoil proton generation to broad energy neutron spectrum, like the one of the ^{241}AmBe source (Sykora et al., 2008b; Stabilini et al., 2021b; Becker et al., 2022). Instead, fewer dedicated studies have been performed on mono-energetic neutron beams. For instance, Fomenko et al. (2018) used a PE converter with a thickness of 0.72 mm for the measurement of mono-energetic neutrons up to 16.5 MeV. They concluded the results obtained for neutron energies below 5 MeV cannot be extrapolated for describing the FNTDs response to higher neutron energies.

For mono-energetic neutrons, the obtained results revealed the need for larger PE converter thicknesses when increasing the neutron energy used (Fig. 5). Moreover, the results indicate that a converter thickness of 4 mm might be a good compromise to measure even 19 MeV neutrons with a sensitivity loss of approximately 3 % for 5 MeV neutrons.

4.4. Accuracy improvement by other techniques

For further detector analysis, different techniques could be considered, such as the use of polytetrafluoroethylene (PTFE) as a converter material to correct for the gamma signal contribution (Akselrod and Sykora, 2011). Using this technique, the offset shown in Fig. 3 might be reduced. Also, the application of the Principle Component Analysis (PCA) and the use of different information from the track spots, like circularity and mean intensity, could be beneficial in terms of neutron dose contribution discrimination (Stabilini et al., 2021a).

Other techniques for readout and post-processing include 3D tracking, which enables assessment of recoil tracks and might further reduce the uncertainty (Stabilini et al., 2020). LET determination could further advance the post-processing and would be advantageous for the application in secondary neutron dose estimation, allowing discrimination between primary particles, fragments and recoil protons. A similar technique has been introduced for PNTD detectors (Caresana et al., 2012). In combination with proper positioning of the detectors, secondary neutron dose determination could be improved (Vedelago et al., 2022). Further attempts to reduce the uncertainty could also be done by introducing correction methods for the FNTD colouration (Muñoz et al., 2022; Kusumoto et al., 2023). Applying these techniques might help to improve the accuracy of the results presented in Figs. 3 and 4.

4.5. Implications for secondary neutron detection in ion beam radiotherapy

As indicated in Fig. 5b, the sensitivity for higher neutron energies increases at a slower rate than the rise in required PE converter thickness. This trend might become even more pronounced for the application of FNTD technology in IBRT when measuring secondary neutrons. Since the thickness of converters may be limited in certain configurations and settings, other converter materials might be required to further increase the sensitivity. For example, in rem counter detectors, high Z materials such as lead or tungsten are employed to improve the sensitivity for neutron energies up to hundreds of MeV (Olsher and McLean, 2008). Therefore, further steps will include the measurement of neutrons with energies up to and above 20 MeV, complemented with a study of different converter configurations and materials suitable for the high-energy neutrons present in IBRT facilities.

In addition, secondary neutron spectra from proton and other ion beams, as presented by Vedelago et al. (2022) and Geser et al. (2024), could be used for assessing the performance of converters by conducting MC simulations, considering the energy distribution of these neutrons. Resulting values can then be compared with secondary neutron dose measurements reported in other studies for primary ion beams (Agosteo et al., 1998; Tessa et al., 2014; Stolarczyk et al., 2018).

It should be noted that using the calibration curves presented here for the ^{241}AmBe source directly for higher neutron energies, such as those of the secondary neutrons in IBRT, may result in overestimations of the dose. Therefore, future steps should focus on comparing the MC simulations for neutron energies up to 20 MeV with experimental data. Subsequently, further MC simulations could be used to guide the design of suitable converters for higher neutron energies to cover the full energy spectrum of secondary neutrons produced during IBRT.

Overall, this study represents an initial step towards a characterisation of FNTDs for secondary neutron measurements in IBRT, as it reports the sensitivity of the detectors for neutrons with energies up to 11 MeV through a combination of experiments and MC simulations, and up to 20 MeV by simulations only, covering the energy range of the evaporation peak of secondary neutrons produced during IBRT.

5. Conclusion

Improvements in Fluorescent Nuclear Track Detectors (FNTDs) technology for neutron dosimetry were developed, including optimisation of the readout area, post-irradiation analysis and converter thickness. For a ^{241}AmBe neutron source with a maximum energy of 11 MeV, a readout area of 0.10 mm^2 was found to be optimal for the dedicated FNTD reader, considering a balance between the total uncertainty and the readout area. Additionally, the sensitivity was optimised by testing different converter thicknesses, yielding the highest sensitivity of (22.7 ± 3.4) tracks mSv^{-1} mm^{-2}. The experimental data was used to verify the magnitude of the estimations of a FLUKA Monte Carlo model, which was later used to assess the detector sensitivity at higher neutron energies and to optimise the converter thickness for future experiments involving neutron energies up to 20 MeV. In summary, this study provides the basis for implementing FNTDs for higher neutron energies, as the Monte Carlo simulation can be used for estimating the converter thickness to be later experimentally characterised.

CRediT authorship contribution statement

Stefan Schmidt: Writing – review & editing, Writing – original draft, Visualization, Validation, Software, Methodology, Investigation, Formal analysis, Data curation, Conceptualization. **Alberto Stabilini:** Writing – review & editing, Software. **Long-Yang J. Thai:** Writing – review & editing, Investigation, Formal analysis, Data curation. **Eduardo G. Yukihara:** Writing – review & editing, Supervision. **Oliver Jäkel:** Writing – review & editing, Resources, Conceptualization. **José Vedelago:** Writing – review & editing, Writing – original draft, Supervision, Resources, Project administration, Funding acquisition, Conceptualization.

Declaration of competing interest

The authors declare that they have no known competing financial interests or personal relationships that could have appeared to influence the work reported in this paper.

Data availability

Data will be made available on request.

Acknowledgements

This project was partially financed by the German Research Foundation (Deutsche Forschungsgemeinschaft; DFG) - Project number 495217943. The authors wish to express their gratitude to Armin Runz and Jens Lang from DKFZ for their support in designing and constructing the FNTD holders and providing access to the ^{241}AmBe source.

Appendix A. Supplementary data

Supplementary material related to this article can be found online at https://doi.org/10.1016/j.radmeas.2024.107097.

References

Agosteo, S., Birattari, C., Caravaggio, M., Silari, M., Tosi, G., 1998. Secondary neutron and photon dose in proton therapy. Radiother. Oncol. 48 (3), 293–305. http://dx.doi.org/10.1016/s0167-8140(98)00049-8.

Ahdida, C., Bozzato, D., Calzolari, D., Cerutti, F., Charitonidis, N., Cimmino, A., Coronetti, A., D'Alessandro, G., Servelle, A., Esposito, L., et al., 2022. New capabilities of the FLUKA multi-purpose code. Aip. Conf. Proc. 9, 788253. http://dx.doi.org/10.3389/fphy.2021.788253.

Akselrod, G., Akselrod, M., Benton, E., Yasuda, N., 2006. A novel Al2O3 fluorescent nuclear track detector for heavy charged particles and neutrons. Nucl. Instrum. Methods Phys. Res. B 247 (2), 295–306. http://dx.doi.org/10.1016/j.nimb.2006.01.056.

Akselrod, M.S., Fomenko, V.V., Bartz, J.A., Haslett, T., 2014. Automatic neutron dosimetry system based on fluorescent nuclear track detector technology. Radiat. Prot. Dosim. 161 (1–4), 86–91. http://dx.doi.org/10.1093/rpd/nct293.

Akselrod, M., Kouwenberg, J., 2018. Fluorescent nuclear track detectors - Review of past, present and future of the technology. Radiat. Meas. 117, 35–51. http://dx.doi.org/10.1016/j.radmeas.2018.07.005.

Akselrod, M.S., Sykora, G.J., 2011. Fluorescent nuclear track detector technology - A new way to do passive solid state dosimetry. Radiat. Meas. 46 (12), 1671–1679. http://dx.doi.org/10.1016/j.radmeas.2011.06.018.

Battistoni, G., Boehlen, T., Cerutti, F., Chin, P., Esposito, L., Fass'o, A., Ferrari, A., Lechner, A., Empl, A., Mairani, A., et al., 2015. Overview of the FLUKA code. Ann. Nucl. Med. 82, 10–18. http://dx.doi.org/10.1016/j.anucene.2014.11.007.

Becker, A., Jäkel, O., Vedelago, J., 2022. Intensity threshold variation method in the post-irradiation analysis of Fluorescent Nuclear Track Detectors for neutron dosimetry. Radiat. Phys. Chem. 200, 110257. http://dx.doi.org/10.1016/j.radphyschem.2022.110257.

Caresana, M., Ferrarini, M., Fuerstner, M., Mayer, S., 2012. Determination of LET in PADC detectors through the measurement of track parameters. Nucl. Instrum. Methods Phys. Res. A 683, 8–15. http://dx.doi.org/10.1016/j.nima.2012.04.071.

Colonna, N., Gunsing, F., Käppeler, F., 2018. Neutron physics with accelerators. Prog. Part. Nucl. Phys. 101, 177–203. http://dx.doi.org/10.1016/j.ppnp.2018.02.002.

Domingo, C., de San-Pedro, M., García-Fusté, M., Romero, M., Amgarou, K., Fernández, F., 2013. Estimation of the response function of a PADC based neutron dosimeter in terms of fluence and Hp(10). Radiat. Meas. 50, 82–86. http://dx.doi.org/10.1016/j.radmeas.2012.02.016.

Dreher, C., Combs, S.E., Clinical rationale and indications for particle therapy. 44, 89–104. http://dx.doi.org/10.1159/000486997.

Fomenko, V., Moreno, B., Million, M., Harrison, J., Akselrod, M., 2018. Energy response of fluorescent nuclear trackdetectors of various colorations tomonoenergetic neutrons. Radiat. Prot. Dosim. 180 (1–4), 215–219. http://dx.doi.org/10.1093/rpd/ncx232.

Gambarini, G., Klamert, V., Agosteo, S., Birattari, C., Gay, S., Rosi, G., Scolari, L., 2004. Study of a method based on TLD detectors for in-phantom dosimetry in BNCT. Radiat. Prot. Dosim. 110 (1–4), 631–636. http://dx.doi.org/10.1093/rpd/nch109.

Geser, F.A., Stabilini, A., Christensen, J.B., Muñoz, I.D., Yukihara, E.G., Jaekel, O., Vedelago, J., 2024. A Monte Carlo study on the secondary neutron generation by oxygen ion beams for radiotherapy and its comparison to lighter ions. Phys. Med. Biol. http://dx.doi.org/10.1088/1361-6560/ad0f45.

Gómez-Ros, J., Bedogni, R., Domingo, C., 2023. Personal neutron dosimetry: State-of-the-art and new technologies. Radiat. Meas. 161, 106908. http://dx.doi.org/10.1016/j.radmeas.2023.106908.

GUM 2008, 2008. BIPM, IEC, IFCC, ILAC, ISO, IUPAC, IUPAP, OIML. Evaluation of measurement data — Guide to the expression of uncertainty in measurement. In: Joint Committee for Guides in Metrology. JCGM, Vol. 100, URL: https://www.bipm.org/documents/20126/2071204/JCGM_100_2008_E.pdf/cb0ef43f-baa5-11cf-3f85-4dcd86f77bd6.

ICRP, 1996. ICRP publication 74: Conversion coefficients for use in radiological protection against external radiation. Ann. ICRP 26 (3–4), http://dx.doi.org/10.1016/S0146-6453(96)90010-X.

ICRU, 2002. ICRU report 66: Determination of operational dose equivalent quantities for neutrons. URL: https://www.icru.org/report/determination-of-operational-dose-equivalent-quantities-for-neutrons-report-66.

ISO 8529-1:2021-11, 2021. Reference Neutron Radiations Fields - Part 1: Characteristics and Methods of Production. Standard, International Organization for Standardization, URL: https://www.iso.org/standard/80060.html.

Jäkel, O., Kraft, G., Karger, C.P., 2022. The history of ion beam therapy in Germany. Z. Med. Phys. 32 (1), 6–22. http://dx.doi.org/10.1016/j.zemedi.2021.11.003.

Klimpki, G., Mescher, H., Akselrod, M.S., Jäkel, O., Greilich, S., 2016. Fluence-based dosimetry of proton and heavier ion beams using single track detectors. Phys. Med. Biol. 61 (3), 1021–1040. http://dx.doi.org/10.1088/0031-9155/61/3/1021.

Kusumoto, T., Akselrod, M.S., Harrison, J., Kodaira, S., 2023. Correction method of the coloration in fluorescent nuclear track detector. Radiat. Meas. 161, 106898. http://dx.doi.org/10.1016/j.radmeas.2022.106898.

Mayer, S., Forkel-Wirth, D., Fuerstner, M., Menzel, H.G., Mueller, M.J., Perrin, D., Theis, C., Vincke, H., 2006. Response of neutron detectors to high-energy mixed radiation fields. Radiat. Prot. Dosim. 125 (1–4), 289–292. http://dx.doi.org/10.1093/rpd/ncm182.

Mendoza, E., Cano-Ott, D., 2018. Update of the evaluated neutron cross section libraries for the Geant4 code. http://dx.doi.org/10.61092/iaea.5knd-4xdd.

Mendoza, E., Cano-Ott, D., Guerrero, C., Capote, R., 2012. New evaluated neutron cross section libraries for the GEANT4 code. URL: http://www-nds.iaea.org/publications/indc/indc-nds-0612.pdf.

Mendoza, E., Cano-Ott, D., Koi, T., Guerrero, C., 2014. New standard evaluated neutron cross section libraries for the GEANT4 code and first verification. IEEE Trans. Nucl. Sci. 61 (4), 2357–2364. http://dx.doi.org/10.1109/tns.2014.2335538.

Muñoz, I.D., Burigo, L.N., Gehrke, T., Brons, S., Greilich, S., Jäkel, O., 2022. Sensitivity correction of fluorescent nuclear track detectors using alpha particles: Determining LET spectra of light ions with enhanced accuracy. Med. Phys. 50 (4), 2385–2401. http://dx.doi.org/10.1002/mp.16083.

Nolte, R., Allie, M.S., Bottger, R., Brooks, F.D., Buffler, A., Dangendorf, V., Friedrich, H., Guldbakke, S., Klein, H., Meulders, J.P., et al., 2004. Quasi-monoenergetic neutron reference fields in the energy range from thermal to 200 MeV. Radiat. Prot. Dosim. 110 (1–4), 97–102. http://dx.doi.org/10.1093/rpd/nch195.

Olsher, R.H., Hsu, H.-H., Beverding, A., Kleck, J.H., Casson, W.H., Vasilik, D.G., Devine, R.T., 2000. Wendi: An improved neutron rem meter. Health Phys. 79 (2), 170–181. http://dx.doi.org/10.1097/00004032-200008000-00010.

Olsher, R.H., McLean, T.D., 2008. High-energy response of the PRESCILA and WENDI-II neutron rem meters. Radiat. Prot. Dosim. 130 (4), 510–513. http://dx.doi.org/10.1093/rpd/ncn092.

Pomp, S., Bartlett, D.T., Mayer, S., Reitz, G., Rottger, S., Silari, M., Smit, F.D., Vincke, H., Yasuda, H., 2013. High-energy quasi-monoenergetic neutron fields: existing facilities and future needs. Radiat. Prot. Dosim. 161 (1–4), 62–66. http://dx.doi.org/10.1093/rpd/nct259.

Sbalzarini, I., Koumoutsakos, P., 2005. Feature point tracking and trajectory analysis for video imaging in cell biology. J. Struct. Biol. 151 (2), 182–195. http://dx.doi.org/10.1016/j.jsb.2005.06.002.

Schardt, D., Elsässer, T., Schulz-Ertner, D., 2010. Heavy-ion tumor therapy: Physical and radiobiological benefits. Rev. Mod. Phys. 82 (1), 383. http://dx.doi.org/10.1103/revmodphys.82.383.

Schindelin, J., Arganda-Carreras, I., Frise, E., Kaynig, V., Longair, M., Pietzsch, T., Preibisch, S., Rueden, C., Saalfeld, S., Schmid, B., et al., 2012. Fiji: an open-source platform for biological-image analysis. Nat. Methods 9 (7), 676–682. http://dx.doi.org/10.1038/nmeth.2019.

Schneider, U., Hälg, R., 2015. The impact of neutrons in clinical proton therapy. Front. Oncol. 5, 235. http://dx.doi.org/10.3389/fonc.2015.00235.

Scholz, M., 2000. Heavy ion tumour therapy. Nucl. Instrum. Methods Phys. Res. B 161–163, 76–82. http://dx.doi.org/10.1016/s0168-583x(99)00669-2.

Shrestha, S., Newhauser, W.D., Donahue, W.P., Pérez-Andújar, A., 2022. Stray neutron radiation exposures from proton therapy: physics-based analytical models of neutron spectral fluence, kerma and absorbed dose. Phys. Med. Biol. 67 (12), 125019. http://dx.doi.org/10.1088/1361-6560/ac7377.

Smith, B.R., Hyer, D.E., Hill, P.M., Culberson, W.S., 2019. Secondary neutron dose from a dynamic collimation system during intracranial pencil beam scanning proton therapy: A Monte Carlo investigation. Int. J. Radiat. Oncol. Biol. Phys. 103 (1), 241–250. http://dx.doi.org/10.1016/j.ijrobp.2018.08.012.

Stabilini, A., Akselrod, M., Fomenko, V., Greilich, S., Harrison, J., Yukihara, E., 2020. 3D track reconstruction of neutron-induced recoil protons in fluorescent nuclear track detectors (FNTDs). Radiat. Meas. 137, 106438. http://dx.doi.org/10.1016/j.radmeas.2020.106438.

Stabilini, A., Akselrod, M., Fomenko, V., Harrison, J., Yukihara, E., 2021a. Principal Component Analysis applied to neutron dosimetry based on PADC detectors and FNTDs. Radiat. Meas. 141, 106516. http://dx.doi.org/10.1016/j.radmeas.2021.106516.

Stabilini, A., Kiselev, D., Akselrod, M., Yukihara, E., 2021b. A Monte-Carlo study on the fluorescent nuclear track detector (FNTD) response to fast neutrons: Which information can be obtained by single layer and 3D track reconstruction analyses? Radiat. Meas. 145, 106609. http://dx.doi.org/10.1016/j.radmeas.2021.106609.

Stolarczyk, L., Trinkl, S., Romero-Expósito, M., Mojżeszek, N., Ambrozova, I., Domingo, C., Davídková, M., Farah, J., Kłodowska, M., Knežević, Z., et al., 2018. Dose distribution of secondary radiation in a water phantom for a proton pencil beam—EURADOS WG9 intercomparison exercise. Phys. Med. Biol. 63 (8), 085017. http://dx.doi.org/10.1088/1361-6560/aab469.

Sykora, G.J., Akselrod, M.S., 2010. Novel fluorescent nuclear track detector technology for mixed neutron-gamma fields. Radiat. Meas. 45 (3–6), 594–598. http://dx.doi.org/10.1016/j.radmeas.2010.01.037.

Sykora, G., Akselrod, M., Benton, E., Yasuda, N., 2008a. Spectroscopic properties of novel fluorescent nuclear track detectors for high and low LET charged particles. Radiat. Meas. 43 (2–6), 422–426. http://dx.doi.org/10.1016/j.radmeas.2007.11.009.

Sykora, G., Akselrod, M., Vanhavere, F., 2009. Performance of fluorescence nuclear track detectors in mono-energetic and broad spectrum neutron fields. Radiat. Meas. 44 (9–10), 988–991. http://dx.doi.org/10.1016/j.radmeas.2009.10.027.

Sykora, G., Salasky, M., Akselrod, M., 2008b. Properties of novel fluorescent nuclear track detectors for use in passive neutron dosimetry. Radiat. Meas. 43 (2–6), 1017–1023. http://dx.doi.org/10.1016/j.radmeas.2007.12.038.

Tanner, R., Bartlett, D., Hager, L., 2005. Operational and dosimetric characteristics of etched-track neutron detectors in routine neutron radiation protection dosimetry. Radiat. Meas. 40 (2–6), 549–559. http://dx.doi.org/10.1016/j.radmeas.2005.01.016.

Tessa, C.L., Berger, T., Kaderka, R., Schardt, D., Burmeister, S., Labrenz, J., Reitz, G., Durante, M., 2014. Characterization of the secondary neutron field produced during treatment of an anthropomorphic phantom with x-rays, protons and carbon ions. Phys. Med. Biol. 59 (8), 2111–2125. http://dx.doi.org/10.1088/0031-9155/59/8/2111.

The MathWorks Inc., 2023. MATLAB version: 9.14.0 (R2023a). URL: https://www.mathworks.com.

Toppi, M., Battistoni, G., Bochetti, A., De Maria, P., De Simoni, M., Dong, Y., Fischetti, M., Franciosini, G., Gasparini, L., Magi, M., et al., 2020. The MONDO tracker: Characterisation and study of secondary ultrafast neutrons production in carbon ion radiotherapy. Aip. Conf. Proc. 8, 567990. http://dx.doi.org/10.3389/fphy.2020.567990.

Van Hoey, O., Stolarczyk, L., Lillhök, J., Eliasson, L., Mojzeszek, N., Liszka, M., Alkhiat, A., Mares, V., Trompier, F., Trinkl, S., et al., 2022. Simulation and experimental verification of ambient neutron doses in a pencil beam scanning proton therapy room as a function of treatment plan parameters. Front. Oncol. 12, 903537. http://dx.doi.org/10.3389/fonc.2022.903537.

Vanhavere, F., Loos, M., Plompen, A., Wattecamps, E., Thierens, H., 1998. A combined use of the BD-PND and BDT bubble detectors in neutron dosimetry. Radiat. Meas. 29 (5), 573–577. http://dx.doi.org/10.1016/S1350-4487(98)00071-7.

Vedelago, J., Geser, F.A., Muñoz, I.D., Stabilini, A., Yukihara, E.G., Jäkel, O., 2022. Assessment of secondary neutrons in particle therapy by Monte Carlo simulations. Phys. Med. Biol. 67 (1), 015008. http://dx.doi.org/10.1088/1361-6560/ac431b.

Vlachoudis, V., 2009. Flair: A powerful but user friendly graphical interface for FLUKA. In: Proc. Int. Conf. on Mathematics, Computational Methods & Reactor Physics, Saratoga Springs, New York. Vol. 2, URL: https://flair.web.cern.ch/flair/doc/Flair_MC2009.pdf.

Wang, Y.-H., Li, Q., Chen, L., Yuan, Y.-G., Peng, T.-P., 2019. Simulation study of the dose and energy responses of FNTD personal neutron dosimetry. Nucl. Sci. Tech. 30, 32. http://dx.doi.org/10.1007/s41365-019-0546-x.

Wilson, R.R., 1946. Radiological use of fast protons. Radiology 47 (5), 487–491. http://dx.doi.org/10.1148/47.5.487.

Yukihara, E.G., Akselrod, M.S., Fomenko, V., Harrison, J., Million, M., Assenmacher, F., Stabilini, A., Meier, K., 2017. Comparison between padc and fntd neutron detector systems in blind tests. Radiat. Prot. Dosim. 180 (1–4), 225–229. http://dx.doi.org/10.1093/rpd/ncx171.